Hedgehog-Like Upconversion Crystals: Controlled Growth and Molecular Sensing at Single-Particle Level

Xiaowang Liu, Xiyan Li, Xian Qin, Xiaoji Xie, Ling Huang, and Xiaogang Liu**

Topological control of nanostructures plays a crucial role in understanding the crystal growth process at the nanometer length scale. Here, the scalable synthesis of upconversion materials with distinct hedgehog-like morphologies by a seed-mediated synthetic procedure is reported. It is demonstrated that a close match in the crystal lattice between the core and shell components is essential for synthesizing such hierarchical nanostructures. These optical nanomaterials also enable the development of a single-particle-based platform for high-sensitivity molecular sensing.

Hierarchical nanostructures, built upon controlled assembly of nanoscale elements into 3D structures with precise size and morphology, have been widely studied in the past decade.[1] Hierarchical nanostructuring offers a set of benefits, including high surface-to-volume ratio and the possibility of multifunctionalization imparted by a synergistic interaction between constituting components.[2] These benefits have led to the development of numerous applications in the fields of catalysis, photonics, sensing, and energy conversion.[3] For example, hierarchical Si/InGaN nanowires with a core–shell structure enable much improved photoelectrochemical performance in water splitting due to extended range for light absorption as well as enhanced charge separation and transportation, as opposed to InGaN nanowires alone.[4]

The ability to control the topology and composition diversity in hierarchical nanostructures is thus essential to enrich their optical, magnetic, and electronic properties for use in a particular field. Previous studies revealed that the major building blocks constituting the hierarchical system should have a low lattice mismatch, typically less than 7%.[5] Sodium rare-earth fluorides ($NaLnF_4$) are ideal for such applications because of their resemblance in lattice structure. For example, the lattice mismatch in hexagonal-phased $NaGdF_4$ and $NaY(Lu)F_4$ crystals is only less than 3% (Table S1 and S2, Supporting Information). Additionally, $NaLnF_4$ host materials have proven effective in accommodating a large variety of lanthanide dopants with easily adjustable concentrations.[6] This particular attribute has led to the preparation of an intriguing class of materials termed upconversion nanocrystals. In effect, such optical nanomaterials hold great promise in the fields of biosensing and bioimaging largely due to their large anti-Stokes emission and the elimination of background autofluorescence when excited with a near-infrared source of light.[7] We reason that the development of hierarchical structuring in upconversion crystals might bestow a new set of materials functionality for bioapplications. Herein, we report a chemical route toward preparing hedgehog-like upconversion microsized and nanosized particles. Interestingly, this hedgehog structure enables a high density, uniform surface modification of the particles with a thin layer of MnO_2. We further demonstrate that these MnO_2-modified hedgehog particles are especially useful for rapid detection of dithiothreitol (DTT) with single-particle sensitivity.

We at first carried out the growth of $NaGdF_4$:Yb/Tm (49/1 mol%) crystals on the surface of $NaYF_4$:Yb/Er (18/2 mol%) microrods as a model system to demonstrate a hierarchical control over upconversion nanostructures (**Figure 1**a and Figure S1 and S2, Supporting Information). The shell matrix of $NaGdF_4$:Yb/Tm (49/1 mol%) was in situ generated by thermal decomposition of a mixture of lanthanide and sodium trifluoroacetates at a high temperature (310 °C).[8]

Transmission electron microscopy (TEM) of the as-synthesized microrods shows a highly ordered structure, and a closer inspection indicates that the shell layer is formed by well-aligned nanorod arrays (Figure 1b,c). Energy-dispersive X-ray spectroscopy (EDX) analysis confirms the core–shell morphology of the resulting microstructures according to element mapping (Figure 1c, insets) and line scanning analysis (Figure S3, Supporting Information). Powder X-ray diffraction (XRD) characterization reveals that both the core and shell components are in the form of hexagonal phase and highly crystalline in nature (Figure S2, Supporting Information). These results are in line with high-resolution TEM characterization (Figure 1d). The observed *d* spacings of 0.30 nm from the two components were confirmed to be interplanar distances of the $(11\bar{2}\ 0)$ planes for hexagonal $NaYF_4$ and $NaGdF_4$, respectively. The well alignment of these lattice fringes at the

Dr. X. Liu, Dr. X. Li, Dr. X. Qin, Prof. X. Liu
Department of Chemistry
National University of Singapore
Singapore 117543, Singapore
E-mail: chmlx@nus.edu.sg
Dr. X. Xie, Prof. L. Huang
Key Laboratory of Flexible Electronics & Institute of Advanced Materials
Jiangsu National Synergetic Innovation Center for Advanced Materials
Nanjing Tech University
Nanjing 211816, P. R. China
E-mail: iamlhuang@njtech.edu.cn
Prof. X. Liu
Center for Functional Materials
NUS (Suzhou) Research Institute
Suzhou, Jiangsu 215123, P. R. China
The ORCID identification number(s) for the author(s) of this article can be found under https://doi.org/10.1002/adma.201702315.

DOI: 10.1002/adma.201702315

 © 2017 WILEY-VCH Verlag GmbH & Co. KGaA, Weinheim

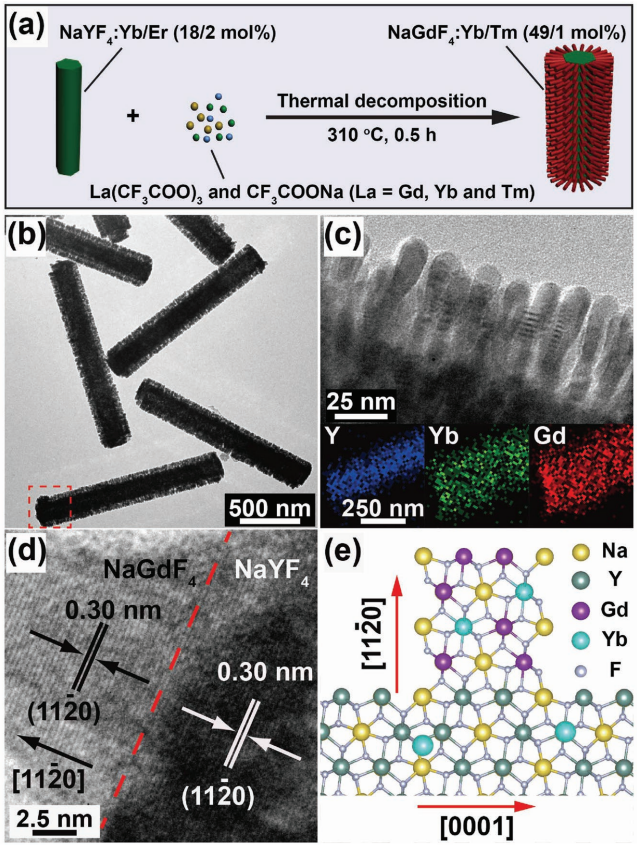

Figure 1. a) Experimental design for the synthesis of hierarchical upconversion microcrystals. b) Representative TEM image of the as-synthesized $NaYF_4$:Yb/Er(18/2 mol%)@$NaGdF_4$:Yb/Tm(49/1 mol%) microcrystals. c) TEM imaging showing the hierarchical structure of the sample. Insets: EDX elemental mappings of the tip of a selected microcrystal marked in (b). d) High-resolution TEM image of the microcrystal. e) Schematic lattice construction of the epitaxial growth of $NaGdF_4$:Yb/Tm over $NaYF_4$:Yb/Er template.

interface implies the epitaxial growth relationship between the $NaGdF_4$ nanorods and the $NaYF_4$ microrods (Figure 1e).[9]

In a further set of control experiments, we examined the experimental parameters that may exert a profound impact on the hierarchical growth of $NaGdF_4$:Yb/Tm shell onto the $NaYF_4$:Yb/Er core. We found that a decrease in temperature-rising rate from 12 to 4.5 °C min^{-1} can also give rise to hedgehog-like hierarchical microstructures (Figure S4a, Supporting Information). However, a pronounced decline in the population of the secondary structure was observed, accompanied with a slight increase in the length of the nanorods (≈15 nm). This observation reflects the formation of a less amount of active sites on the core microrods at a slower rate of temperature rise, thereby leading to a slow growth in shell lattice and hence the yield of nanorods with large aspect ratios. As expected, control experiments with parameters that affect the nucleation kinetics of the shell matrix showed the lack of control over the morphology of ultimately formed microstructures. For example, lowering the molar ratio of sodium-to-lanthanide precursor in the mother solution from 1.8:1 to 1:1 (Figure S4b, Supporting Information) or reducing the molar ratio of shell precursor-to-particle seed from 8:1 to 2:1 (Figure S5a, Supporting Information) did not yield any hierarchical microstructures. Notably, a large decrease in the amount of shell precursor can even lead to a ligand-assisted etching to $NaYF_4$ microrods (Figure S5b, Supporting Information).[10] As a separate note, the hierarchical structures of the resulting microrods could not be accessed by coprecipitation and hydrothermal methods (Figure S6, Supporting Information), in which thermal dynamic factors mainly control the reactions.[11] Taken together, these findings suggest that the kinetic control plays a dominant role in regulating the hierarchical morphology.

To understand the kinetics of shell growth, we performed time-dependent TEM analysis of the as-prepared hierarchical microrods. Our results suggest that the shell precursor starts decomposing at a temperature of about 270 °C and the process of decomposition completes within 2 min (**Figure 2**a). The rapid rate of decomposition was made evident by the observation of a burst production of gas bubbles in the solution at 270 °C (Figure 2b). As a result, we noticed a marginal change in the morphology of the as-synthesized core–shell microstructures obtained in the temperature range from 270 to 310 °C (Figure 2c). Interestingly, subsequent heating of the product solution at 310 °C for 30 minutes led to the formation of low-density nanorods on the surface of the microrod templates. This phenomenon is likely caused by Ostwald ripening, which are driven by a tendency to minimize the exposed surface areas of the microrods under study (Figure 2d–f).[12] These findings suggest that the thermodynamic control comes into play at the late stage of crystal growth.

As the dimension of the as-synthesized microrods exceeds the diffraction limit of visible light, their optical properties can

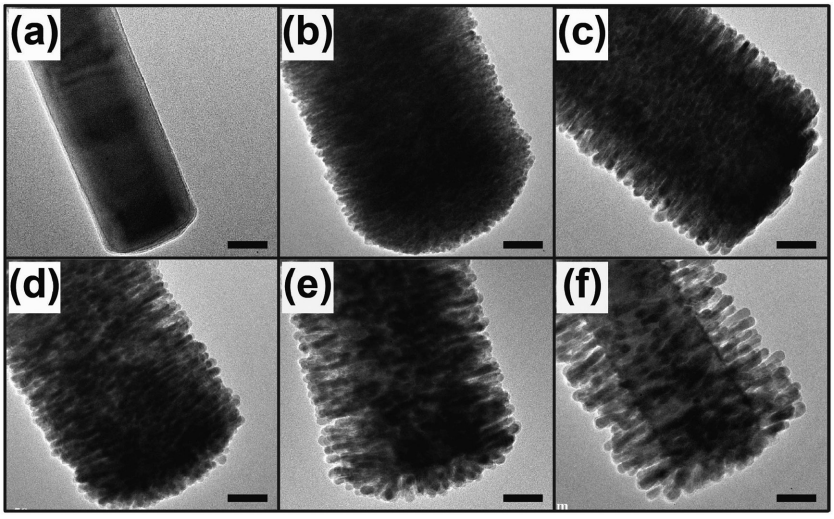

Figure 2. TEM images of hierarchical microcrystals obtained at different temperatures and reaction times. a–c) The reaction temperature is set at 260, 270, and 310 °C, respectively. d–f) The time interval is set at 10, 20, and 30 min, respectively. Scale bars are 100 nm.

© 2017 WILEY-VCH Verlag GmbH & Co. KGaA, Weinheim

be readily probed at a single-particle level through wide-field luminescence microscopy. When irradiated at 980 nm, a single $NaYF_4$:Yb/Er (18/2 mol%) microrod exhibited a characteristic green emission, corresponding to the optical transitions of $^2H_{11/2}\rightarrow{}^4I_{15/2}$, $^4S_{3/2}\rightarrow{}^4I_{15/2}$, and $^4F_{9/2}\rightarrow{}^4I_{15/2}$ of Er^{3+} (Figure S7a, inset, Supporting Information).[13] After coating of a layer of $NaGdF_4$:Yb/Tm (49/1 mol%) nanorods, the emission color of the microrod under investigation turned whitish because of the mixing of both Er^{3+} and Tm^{3+} emissions (Figure S7b, inset, Supporting Information). Meanwhile, we observed a rise in the lifetime of Er^{3+} emission at 542 nm from 178 to 438 µs (Figure S8, Supporting Information), suggesting the protection effect of the hierarchical shell layer.[14]

It is worth noting that the kinetically controlled procedure has considerable robustness in yielding a variety of hierarchical morphologies onto different core particles (Figure S9, Supporting Information). These include $NaYF_4$:Gd, $NaYbF_4$:Gd, and $NaGdF_4$:Yb/Tm particles (**Figure 3**a–c). Interestingly, the use of spherical nanoparticles ($NaGdF_4$:Yb/Tm@$NaGdF_4$:Tb) or nanoplates ($NaGdF_4$ and $NaYbF_4$) for shell growth led to urchin-like core–shell nanostructures (Figure 3d–f). In addition, different shell matrices, such as $NaGdF_4$ and $NaYbF_4$ (Figure S10, Supporting Information), are applicable for the synthesis of hierarchical core–shell structures. However, the attempt to grow $NaScF_4$ on $NaYF_4$ microrods failed due to phase separation (Figure S11, Supporting Information). These results suggest that lattice compatibility between core and shell matrices also significantly contributes to hierarchical growth in the synthesis of hedgehog-like upconversion crystals via a seed-mediated procedure (Table S3, Supporting Information).[15]

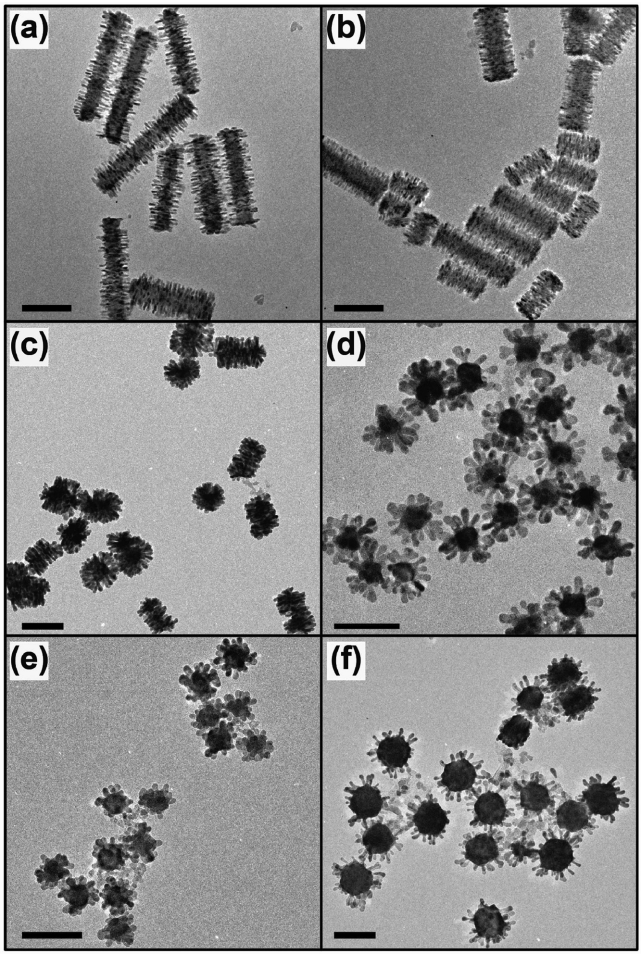

Figure 3. Representative TEM images of hierarchical core–shell nanostructures prepared using different types of seeding particles: a) $NaYF_4$:Gd (30 mol%), b) $NaYbF_4$:Gd (30 mol%), c) $NaGdF_4$:Yb/Tm (49/1 mol%), d) $NaGdF_4$:Yb/Tm (49/1 mol%)@$NaGdF_4$:Tb (15 mol%), e) $NaGdF_4$, and f) $NaYbF_4$. Scale bars are 200 nm.

The hierarchical nature of our microrods may allow easy surface modification of additional functional materials because of their high surface area as well as rough surface feature. To test this possibility, we prepared ligand-free, hierarchical $NaYF_4$:Yb/Tm@$NaGdF_4$:Yb/Tm microrods and incubated them in an acidic solution of $KMnO_4$ for 12 h at room temperature (**Figure 4**a). We found that a layer of MnO_2 nanosheets is uniformly formed on the microrod templates, and the loading capacity is about 0.28 g/g (Figure 4b, top panel).[15] By comparison, substitution of the hierarchical microrods with smooth-surfaced $NaYF_4$ counterparts as the templates led to a lower MnO_2 loading capacity of 0.09 g/g under identical synthetic conditions (Figure 4b, bottom panel). Note that the low-temperature synthesis also leads to poor crystallinity of the MnO_2 layer (Figure S12a,b, Supporting Information). In addition, the signal arising from the elemental Gd becomes indistinguishable in the EDX profile of the MnO_2-encapsulated $NaYF_4$:Yb/Tm@$NaGdF_4$:Yb/Tm microrods (Figure S12c, Supporting Information), suggesting the occurrence of surface etching of the microrods during the incubation. In fact, the etching ability of the incubation solution was further supported by the observation that the whole $NaYF_4$:Yb/Tm@$NaGdF_4$:Yb/Tm microrods were completely dissolved by slight increase in the acidic level of the incubation mixture, allowing the formation of MnO_2 microcapsules (Figure S13, Supporting Information).

The growth of a dense layer of MnO_2 onto our hierarchical microrods further enables the development of a molecular sensing platform with single-particle detection sensitivity.[16] To demonstrate this concept, we used an as-prepared single $NaYF_4$:Yb/Tm@$NaGdF_4$:Yb/Tm@MnO_2 particle to detect DTT molecules as they are known to have high reactivity toward the disassociation of MnO_2 nanomaterials (Figure 4a; Figure S14, Supporting Information). The reduction product of MnO_2 is likely to be Mn^{2+}, as evidenced by no obvious position change of Mn(2p) peaks in X-ray photoelectron spectroscopic analysis of $NaYF_4$:Yb/Tm@$NaGdF_4$:Yb/Tm@MnO_2 microrods after incubation with DTT at different concentrations (Figure S15, Supporting Information). In our design, upconversion luminescence, initially in a "turned off" state because of the energy transfer from lanthanide emitters to MnO_2 nanosheets (Figure S16, Supporting Information), is only reactivated after addition of DTT molecules. As expected, a luminescence turn-on process was clearly observed after different amounts of DTT molecules were added to the single particle (Figure 4c). Remarkably, we observed a 7-fold enhancement in the upconversion luminescence at 450 nm upon the addition of a trace amount of DTT (5.0 nmol) (Figure 4d, inset). In contrast, a single $NaYF_4$:Yb/Tm microrod only partially coated with MnO_2 nanosheets was confirmed to be unsuitable for high-sensitivity

 © 2017 WILEY-VCH Verlag GmbH & Co. KGaA, Weinheim

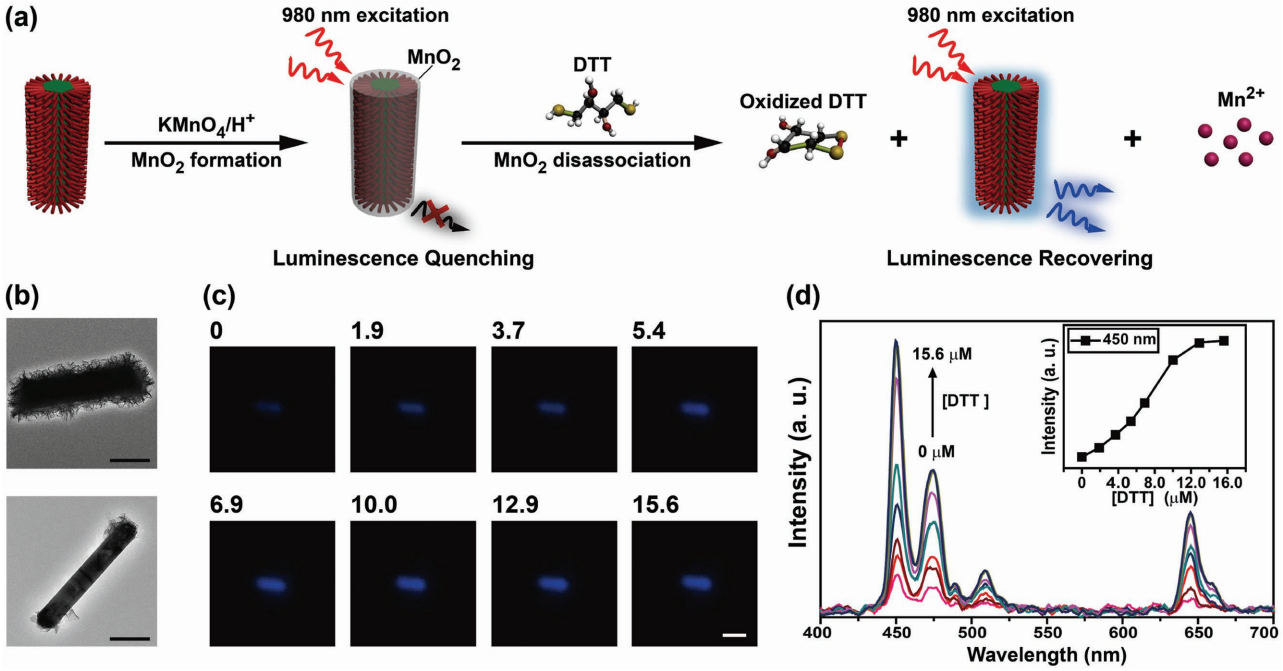

Figure 4. a) Schematic representation illustrating the design of DTT sensing using $NaYF_4$:Yb/Tm(20/0.2 mol%)@$NaGdF_4$:Yb/Tm(49/1 mol%)@MnO_2 microrods. b) TEM imaging of the as-synthesized $NaYF_4$:Yb/Tm(20/0.2 mol%)@$NaGdF_4$:Yb/Tm(49/1 mol%) (top panel) and $NaYF_4$:Yb/Tm (20/0.2 mol%) (bottom panel) particles after overgrowth of MnO_2 under identical experimental conditions (Scale bar: 400 nm). c) Luminescence intensity mapping of a single particle at different concentrations of DTT (0, 1.9, 3.7, 5.4, 6.9, 10.0, 12.9, and 15.6 μm) (Scale bar: 1 μm). d) Corresponding luminescence profiles obtained for the single particle as shown in (c). Insert is the plot of luminescence intensity at 450 nm as a function of DTT concentration.

sensing of DTT. This control showed a negligible change in luminescence signal after the same amount of DTT molecules (5.0 nmol) was added (Figure S17, Supporting Information). The discrepancy in sensitivity is largely attributed to the low loading density of MnO_2 on the particle's surface, which exerts a weak quenching effect on the upconversion luminescence.

Our single-particle-based platform can be used to detect DTT molecules with a concentration as low as ≈1.9 μm, and the calculated detection limit was estimated to be 0.75 μm with a signal-to-noise ratio of 3:1 by comparing measured signals from the samples under study with those of blank control.[17] Note that the obtained detection limit is about two orders of magnitude lower than that attainable from a conventional method involving the use of MnO_2-encapsulated colloidal solutions (Figure S18, Supporting Information). In addition, the detection limit is about 250 times higher than that reported through the use of DNA-coupled MnO_2 nanosheets.[16b] The high sensitivity displayed by the single-particle platform is ascribed to the fact that it requires a much less amount of DTT molecules to reactivate the luminescence as opposed to the conventional methods. Notably, the absence of background emission noise when excited at 980 nm may also partially contribute to the high-sensitivity sensing.[18] The single-particle analytical platform also displayed a considerable selectivity toward DTT. The addition of a variety of molecules or electrolytes (0.1 μmol), including glucose, fructose, $ZnCl_2$, $NaSO_4$, NaCl, $MnCl_2$, KCl, and phosphate-buffered saline, led to marginable signal changes (Figure S19, Supporting Information). Moreover, in situ luminescence studies showed that the platform at work exhibits a rapid optical response, as supported by the observation of a turn-on luminescence within 5 s after the addition of DTT molecules.

In conclusion, we have demonstrated a seed-mediated strategy for controlling hierarchical core–shell structuring over upconversion microcrystals or nanocrystals. The implementation of a kinetically controlled reaction and a lattice-matching scheme between the core and shell components facilitates the formation of hedgehog-like particles. Importantly, this unique secondary structure provides a robust platform for high-density anchoring of MnO_2 nanosheets. The hierarchical multilayer nature of the structure further enables the development of a single-particle-based optical sensing platform for ultralow-concentration DTT molecules. Considering the appealing attributes of upconversion materials, the precise control over their hierarchical complexity presented herein is likely to offer new opportunities for investigating energy transfer dynamics on unprecedented spatial and temporal scales.

Experimental Section

Experimental details and characterization of as-prepared nano-/micromaterials are available in the Supporting Information.

Supporting Information

Supporting Information is available from the Wiley Online Library or from the author.

© 2017 WILEY-VCH Verlag GmbH & Co. KGaA, Weinheim

Acknowledgements

This work was supported by the National Research Foundation, Prime Minister's Office, Singapore under its Competitive Research Program (CRP Award No. NRF-CRP15-2015-03), the National Natural Science Foundation of China (NSFC21471109), and the Natural Science Foundation of Jiangsu Province (ZXG201412 and BE2015699).

Conflict of Interest

The authors declare no conflict of interest.

Keywords

epitaxial growth, hierarchical control, kinetic synthesis, single-particle sensors, upconversion

Received: April 25, 2017
Revised: June 29, 2017
Published online: August 14, 2017

[1] a) T. Zhang, W. Dong, M. Keeter-Brewer, S. Konar, R. N. Njabon, Z. R. Tian, *J. Am. Chem. Soc.* **2006**, *128*, 10960; b) K. Sun, Y. Jing, N. Park, C. Li, Y. Bando, D. Wang, *J. Am. Chem. Soc.* **2010**, *132*, 15465; c) W.-Q. Wu, Y.-F. Xu, H.-S. Rao, C.-Y. Su, D.-B. Kuang, *J. Am. Chem. Soc.* **2014**, *136*, 6437; d) J. Y. Zheng, Y. Yan, X. Wang, Y. S. Zhao, J. Huang, J. Yao, *J. Am. Chem. Soc.* **2012**, *134*, 2880.

[2] a) B. Xu, P. He, H. Liu, P. Wang, G. Zhou, X. Wang, *Angew. Chem., Int. Ed.* **2014**, *53*, 2339; b) T. L. Sounart, J. Liu, J. A. Voigt, M. Huo, E. D. Spoerke, B. McKenzie, *J. Am. Chem. Soc.* **2007**, *129*, 15786; c) J. Zhao, J. Chen, S. Xu, M. Shao, Q. Zhang, F. Wei, J. Ma, M. Wei, D. G. Evans, X. Duan, *Adv. Funct. Mater.* **2014**, *24*, 2938.

[3] W.-Q. Wu, Y.-F. Xu, H.-S. Rao, H.-L. Feng, C.-Y. Su, D. B. Kuang, *Angew. Chem., Int. Ed.* **2014**, *53*, 4816.

[4] Y. J. Hwang, C. H. Wu, C. Hahn, H. E. Jeong, P. Yang, *Nano Lett.* **2012**, *12*, 1678.

[5] a) S. H. Ko, D. Lee, H. W. Kang, K. H. Nam, J. Y. Yeo, S. J. Hong, C. P. Grigoropoulos, H. J. Sung, *Nano Lett.* **2011**, *11*, 666; b) S. Sun, G. Meng, G. Zhang, L. Zhang, *Cryst. Growth Des.* **2007**, *7*, 1988; c) H. G. Yang, H. C. Zeng, *J. Am. Chem. Soc.* **2005**, *127*, 270; d) D.-F. Zhang, L.-D. Sun, C.-J. Jia, Z.-G. Yan, L.-P. You, C.-H. Yan, *J. Am. Chem. Soc.* **2005**, *127*, 13492; e) J. Y. Lao, J. G. Wen, Z. F. Ren, *Nano Lett.* **2002**, *2*, 1287.

[6] a) M. Haase, H. Schäfer, *Angew. Chem., Int. Ed.* **2011**, *50*, 5808; b) H. H. Gorris, O. S. Wolfbeis, *Angew. Chem., Int. Ed.* **2013**, *52*, 3584; c) L. Sun, Y. Wang, C. Yan, *Acc. Chem. Res.* **2014**, *47*, 1001; d) J. H. Hao, Y. Zhang, X. H. Wei, *Angew. Chem., Int. Ed.* **2011**, *50*, 6876; e) S. Gai, C. Li, P. Yang, J. Lin, *Chem. Rev.* **2014**, *114*, 2343; f) J. Lai, B. P. Shah, Y. Zhang, L. Yang, K.-B. Lee, *ACS Nano* **2015**, *9*, 5234; g) L. Li, R. Zhang, L. Yin, K. Zheng, W. Qin, P. R. Selvin, Y. Lu, *Angew. Chem., Int. Ed.* **2012**, *51*, 6121; h) L. Li, Y. Lu, *J. Am. Chem. Soc.* **2015**, *137*, 5272; i) L. H. Fischer, G. S. Harms, O. S. Wolfbeis, *Angew. Chem., Int. Ed.* **2011**, *50*, 4546; j) Y. Dai, H. Xiao, J. Liu, Q. Yuan, P. Ma, D. Yang, C. Li, Z. Cheng, Z. Hou, P. Yang, J. Lin, *J. Am. Chem. Soc.* **2013**, *135*, 18920; k) X. Qin, X. W. Liu, W. Huang, M. Bettinelli, X. Liu, *Chem. Rev.* **2017**, *117*, 4488; l) M. Bettinelli, L. Carlos, X. Liu, *Phys. Today* **2015**, *68*, 38.

[7] a) J. Zhou, Z. Liu, F. Li, *Chem. Soc. Rev.* **2012**, *41*, 1323; b) Z. Li, S. Lv, Y. Wang, S. Chen, Z. Liu, *J. Am. Chem. Soc.* **2015**, *137*, 3421; c) J. Zhao, D. Jin, E. P. Schartner, Y. Lu, Y. Liu, A. V. Zvyagin, L. Zhang, J. M. Dawes, P. Xi, J. A. Piper, E. M. Goldys, T. M. Monro, *Nat. Nanotechnol.* **2013**, *8*, 729; d) Y. Yang, Q. Shao, R. Deng, C. Wang, X. Teng, K. Cheng, Z. Cheng, L. Huang, Z. Liu, X. Liu, B. Xing, *Angew. Chem., Int. Ed.* **2012**, *51*, 3125; e) P. Huang, W. Zheng, S. Zhou, D. Tu, Z. Chen, H. Zhu, R. Li, E. Ma, M. Huang, X. Chen, *Angew. Chem., Int. Ed.* **2014**, *53*, 1252; f) Y. Liu, D. Tu, H. Zhu, X. Chen, *Chem. Soc. Rev.* **2013**, *42*, 6924; g) H. Wen, H. Zhu, X. Chen, T. F. Hung, B. Wang, G. Zhu, S. F. Yu, F. Wang, *Angew. Chem., Int. Ed.* **2013**, *52*, 13419; h) Y. Ding, F. Wu, Y. Zhang, X. Liu, E. M. L. D. de Jong, T. Gregorkiewicz, X. Hong, Y. Liu, M. C. G. Aalders, W. J. Buma, H. Zhang, *J. Phys. Chem. Lett.* **2015**, *6*, 2518.

[8] a) H. Mai, Y. Zhang, R. Si, Z. Yan, L. Sun, L. You, C. Yan, *J. Am. Chem. Soc.* **2006**, *128*, 6426; b) J.-C. Boyer, F. Vetrone, L. A. Cuccia, J. A. Capobianco, *J. Am. Chem. Soc.* **2006**, *128*, 7444; c) F. Wang, L.-D. Sun, J. Gu, Y.-F. Wang, W. Feng, Y. Yang, J. Wang, C.-H. Yan, *Angew. Chem., Int. Ed.* **2012**, *51*, 8796.

[9] M. N. Mankin, R. W. Day, R. Gao, Y.-S. No, S.-K. Kim, A. A. McClelland, D. C. Bell, H.-G. Park, C. M. Lieber, *Nano Lett.* **2015**, *15*, 4776.

[10] C. Zhang, J. Y. Lee, *ACS Nano* **2013**, *7*, 4393.

[11] Y. Zhang, L. Zhang, R. Deng, J. Tian, Y. Zong, D. Jin, X. Liu, *J. Am. Chem. Soc.* **2014**, *136*, 4893.

[12] N. J. J. Johnson, A. Korinek, C. Dong, F. C. J. M. van Veggel, *J. Am. Chem. Soc.* **2012**, *134*, 11068.

[13] a) X. Liu, R. Deng, Y. Zhang, Y. Wang, H. Chang, L. Huang, X. Liu, *Chem. Soc. Rev.* **2015**, *44*, 1479; b) Y. Liu, D. Wang, J. Shi, Q. Peng, Y. Li, *Angew. Chem., Int. Ed.* **2013**, *52*, 4366; c) Y. Xiao, L. Zeng, T. Xia, Z. Wu, Z. Liu, *Angew. Chem., Int. Ed.* **2015**, *54*, 5323; d) P. Lederhose, Z. Chen, R. Müller, J. P. Blinco, S. Wu, C. Barner-Kowollik, *Angew. Chem., Int. Ed.* **2016**, *55*, 12195.

[14] a) C. Drees, A. N. Raj, R. Kurre, K. B. Busch, M. Haase, J. Piehler, *Angew. Chem., Int. Ed.* **2016**, *55*, 11668; b) F. Wang, R. Deng, J. Wang, H. Wang, Y. Han, H. Zhu, X. Chen, X. Liu, *Nat. Mater.* **2011**, *10*, 968; c) M. He, X. Pang, X. Liu, B. Jiang, Y. He, H. Snaith, Z. Lin, *Angew. Chem., Int. Ed.* **2016**, *55*, 4280; d) T. Rinkel, A. N. Raj, S. Dühnen, M. Haase, *Angew. Chem., Int. Ed.* **2016**, *55*, 1164; e) X. Li, Z. Guo, T. Zhao, Y. Lu, L. Zhou, D. Zhao, F. Zhang, *Angew. Chem., Int. Ed.* **2016**, *55*, 2464.

[15] X. Teng, Y. Zhu, W. Wei, S. Wang, J. Huang, R. Naccache, W. Hu, A. I. Y. Tok, Y. Han, Q. Zhang, Q. Fan, W. Huang, J. A. Capobianco, L. Huang, *J. Am. Chem. Soc.* **2012**, *134*, 8340.

[16] a) R. Deng, X. Xie, M. Vendrell, Y. Chang, X. Liu, *J. Am. Chem. Soc.* **2011**, *133*, 20168; b) Z. Zhao, H. Fan, G. Zhou, H. Bai, H. Liang, R. Wang, X. Zhang, W. Tan, *J. Am. Chem. Soc.* **2014**, *136*, 11220; c) X. Zhang, C. Zheng, S. Guo, J. Li, H. Yang, G. Chen, *Anal. Chem.* **2014**, *86*, 3426; d) J. Yuan, Y. Cen, X. Kong, S. Wu, C. Liu, R. Yu, X. Chu, *ACS Appl. Mater. Interfaces* **2015**, *7*, 10548; e) W. Fan, W. Bu, B. Shen, Q. He, Z. Cui, Y. Liu, X. Zheng, K. Zhao, J. Shi, *Adv. Mater.* **2015**, *27*, 4155; f) J. Liu, Y. Liu, W. Bu, J. Bu, Y. Sun, J. Du, J. Shi, *J. Am. Chem. Soc.* **2014**, *136*, 9701.

[17] a) M.-K. Tsang, W. Ye, G. Wang, J. Li, M. Yang, J. Hao, *ACS Nano* **2016**, *10*, 598; b) W. Ye, M.-K. Tsang, X. Liu, M. Yang, J. Hao, *Small* **2014**, *10*, 2390.

[18] a) X. Li, F. Zhang, D. Zhao, *Chem. Soc. Rev.* **2015**, *44*, 1346; b) W. Zheng, P. Huang, D. Tu, E. Ma, H. Zhu, X. Chen, *Chem. Soc. Rev.* **2015**, *44*, 1379.

 © 2017 WILEY-VCH Verlag GmbH & Co. KGaA, Weinheim